

Our EXAFS data have given a direct evidence for a local ordering in the highly concentrated  $\text{CuBr}_2$  aqueous solutions. The elementary unit—a bromine rectangle with a copper at its center—is the same as that of  $\text{CuBr}_2$  crystals. The distorted-rectangular unit suggests that these units are linked together by their smaller side, and form chains like in the crystal. However, the EXAFS experiments cannot give any indication concerning their lengths, and their eventual stacking. The dynamic or static disorder is a little bit larger than in the crystal. It must be pointed out that this disorder increases continuously when the solution is diluted.

Even in dilute solutions ( $c \sim 0.1M$ ) we have an evidence that half of the  $\text{Cu}^{++}$  and  $\text{Br}^-$  ions are not simple hydrated ions but form complex molecules which could be plane square ( $\text{CuBr}_4$ )<sup>2-</sup> anions or  $\text{CuBr}_2$  molecules, which is a structural confirmation of the model recently proposed for  $\text{NiCl}_2$  solutions.<sup>4,5</sup>

The data furthermore give a good example of the power of the EXAFS technique (especially when corroborated with other techniques) in studying the detailed structure of aqueous solutions in all concentration ranges.

<sup>(a)</sup> Also at Istituto di Fisica, Università di Parma, Parma, Italy.

<sup>1</sup>P. Eisenberger and B. M. Kincaid, *Chem. Phys. Lett.* **36**, 134 (1975).

<sup>2</sup>D. R. Sandstrom, H. W. Dodgen, and F. W. Lytle, *J. Chem. Phys.* **67**, 2, 473 (1977).

<sup>3</sup>R. A. Howe, W. S. Howells, and J. E. Enderby, *J. Phys. C* **7**, L111 (1974).

<sup>4</sup>M. P. Fontana, G. Maisano, P. Migliardo, and F. Wanderlingh, *Solid State Commun.* **23**, 489 (1977).

<sup>5</sup>G. Maisano, P. Migliardo, F. Wanderlingh, and M. P. Fontana, to be published.

<sup>6</sup>G. Cubiotti, G. Maisano, P. Migliardo, and F. Wanderlingh, to be published.

<sup>7</sup>See D. E. Irish, in *Ionic Interactions*, edited by S. Petrucci (Academic, New York, 1971); of relevance are also spectroscopic studies on molten salts: For this, see the review of V. A. Maroni and E. J. Cairns in *Molten Salts*, edited by G. Marmantov (M. Dekker, New York, 1969). For an overall review of the physical chemistry of strong electrolyte solutions see the monograph by E. A. Guggenheim and R. H. Stokes, *Equilibrium Properties of Aqueous Solutions of Single Strong Electrolytes* (Pergamon, New York, 1969).

<sup>8</sup>Particular care was given to obtain perfectly clear and precipitate-free solutions. The preparation procedures can be found in Refs. 4 and 5. Furthermore, small-angle neutron scattering measurements on the saturated solutions revealed no microcrystals or inhomogeneities of dimensions in the range  $\sim 15$  to  $\sim 150$  Å. The neutron spectra were taken at the Commissariat à l'Énergie Atomique, Saclay (France) reactor in collaboration with Mme Nierlich of the Laboratory Research Staff.

<sup>9</sup>P. A. Lee and G. Beni, *Phys. Rev. B* **15**, 2862 (1977).

<sup>10</sup>R. W. G. Wyckoff, *Crystal Structures* (Interscience, New York, 1965), Vol. 1, p. 345.

## Observation of a $\Lambda_1$ -Symmetry Surface State on Ni(111)

F. J. Himpsel and D. E. Eastman

IBM Thomas J. Watson Research Center, Yorktown Heights, New York 10598

(Received 10 February 1978)

An  $s$ - $p$ -like intrinsic surface state on Ni(111) has been found which has an energy of  $E_i = -0.25$  eV relative to the Fermi energy at  $\bar{\Gamma}$  and lies between the  $L_3$  ( $E_i \approx -0.15$  eV) and  $L_2'$  ( $E_i = -0.9$  eV) bulk states. Its momentum dispersion ( $E$  vs  $\vec{k}_{\parallel}$ ) and  $h\nu$ -dependent photoionization cross section have been determined using angle-resolved photoemission with synchrotron radiation. The existence of this state significantly affects spin-polarized photoemission, chemisorption, band-structure, and exchange-splitting interpretations for Ni.

Nickel is one of the most-studied metals because of its interesting electronic, magnetic, and chemisorption properties. However, many properties are not yet unambiguously understood; e.g., its  $d$ -band structure (experimental widths are narrower than theoretical), magnetic ex-

change splitting, nature of spin-polarized photoemission and field emission, etc. For example, an exchange splitting  $\delta E_{ex} \approx 0.3$  eV has been reported<sup>1</sup> which is much smaller than recent theoretical estimates, while several inconsistent papers interpreting spin-polarized photoemission

data claim that (1) the Stoner-Wohlfarth-Slater (SWS) model for bulk Ni does not work,<sup>2</sup> (2) the SWS model for bulk Ni does work,<sup>3</sup> and (3) the SWS model works for Ni(100), but only if (calculated) intrinsic *d*-like surface states are considered.<sup>4</sup>

We report new angle-resolved photoemission data for Ni(111) obtained with synchrotron radiation which show the existence of a prominent intrinsic surface state of  $\Lambda_1$  symmetry at the Brillouin-zone center  $\bar{\Gamma}$  with an initial energy  $E_i = -0.25$  eV. This surface state disperses downwards in energy with increasing parallel momentum  $\bar{k}_{\parallel}$  in all directions and exhibits an  $h\nu$ -dependent photoionization cross section similar to that we have measured for the *s-p*-like surface state on Cu(111) at  $E_i = -0.4$  eV (at  $\bar{\Gamma}$ ). At low photon energies,  $\varphi + 0.25 \leq h\nu \leq 12$  eV (work function  $\varphi \approx 5.2$  eV), normal emission from this surface state dominates bulk emission. Bulk emission from states near *L* has also been studied by removing the surface state via chemisorption, and a *d*-like state  $L_3$  ( $E_i \approx -0.15$  eV) and *s-p*-like state  $L_2'$  ( $E_i \approx -0.9$  eV) have been determined. This ordering of bulk band levels corresponds to a much smaller exchange splitting ( $\delta E_{ex} < 0.5$  eV) and lower  $L_2'$  energy level than given by recent self-consistent band calculations.<sup>5,6</sup>

Previously, emission from this Ni(111) surface state was incorrectly interpreted as being due to the bulk  $L_{3\uparrow}$  state (placed at  $-0.5$  eV).<sup>1</sup> This led to the estimates of the exchange splitting  $\delta E_{ex} \approx 0.3$  eV and of the energy gap  $\Delta \approx 0.5$  eV between  $E_F$  and the top of the majority-spin *d* band in the SWS model.<sup>1</sup> Our estimate is  $\Delta \approx 0.15$  eV, which is consistent (using a SWS model) with the observed polarity reversal in spin-polarized photoemission near threshold for Ni(111).<sup>2</sup> At photon energies within  $\sim 2$  eV of threshold, surface-state emission makes a large contribution to the total emission and markedly affects the interpretation of spin-polarized photoemission experiments.

For our measurements, we have used a new two-dimensional (2D) display-type electron spectrometer that directly displays the angular intensity distribution of photoelectrons within a selected energy pass band  $\Delta E$  for a cone of emission angles of  $86^\circ$  full width (1.8 sr). This spectrometer permits angle-integrated and angle-resolved photoelectron spectroscopy. LEED (low-energy-electron diffraction), and Auger spectroscopy (AES) to be done on the same sample. An angle-resolved detector permits any escape direction

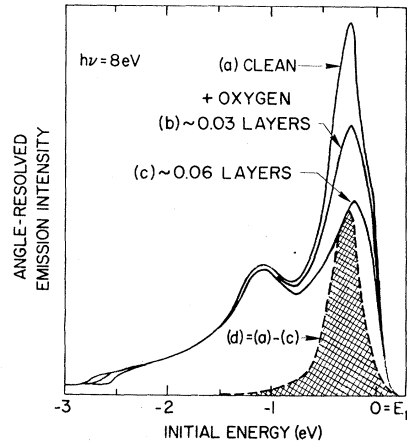


FIG. 1. Angle-resolved energy distributions for emission normal to the surface ( $\delta\theta = 4^\circ$ ) for clean and  $O_2$ -exposed Ni(111). The difference curve *d* shows the surface-state emission.

to be selected with a variable angular acceptance  $1.5^\circ < \delta\theta < 35^\circ$ . Overall energy resolution (photons plus electrons) with monochromated synchrotron radiation from the 240-MeV storage ring at the University of Wisconsin was 100–130 meV for these measurements. The angular acceptance was  $\delta\theta = 4^\circ$  ( $\delta\theta = 2^\circ$  gave similar results). Count rates under these conditions were greater than  $10^4$ /sec for the Ni *d* bands with  $6 \leq h\nu \leq 15$  eV. Ni(111) samples were prepared by Ar-ion etching and annealing in the usual manner, oriented with LEED, and checked for cleanliness by AES in the 2D spectrometer.

In Fig. 1, we present angle-resolved energy distribution curves (AREDC's) with electron emission normal to the surface for (a) clean Ni(111), (b) Ni(111) exposed to 0.5 L (1 L =  $10^{-6}$  Torr sec) of  $O_2$ , (c) Ni(111) exposed to 1.0 L of  $O_2$  (i.e.,  $\approx 1$  monolayer), as well as the change in emission [difference spectrum (d)] to 1 L of  $O_2$  exposure. For Fig. 1, mixed *s-p* polarization and a photon energy of  $h\nu = 8$  eV were used. The dominant peak at  $-0.25$  eV ( $\sim 0.3$  eV full width at half-maximum) is due to an intrinsic surface state which is highly sensitive to adsorbates (oxygen, CO, etc). For example, less than half a monolayer of adsorbed oxygen causes 50% of the surface-state emission to disappear (curve *b*) and submonolayer amounts of residual gas (probably CO) shift its energy downwards. Further evidence for a surface state is that the binding energy of this state for normal emission exhibits no dispersion with changes in photon energy, while bulk transitions disperse with photon energy

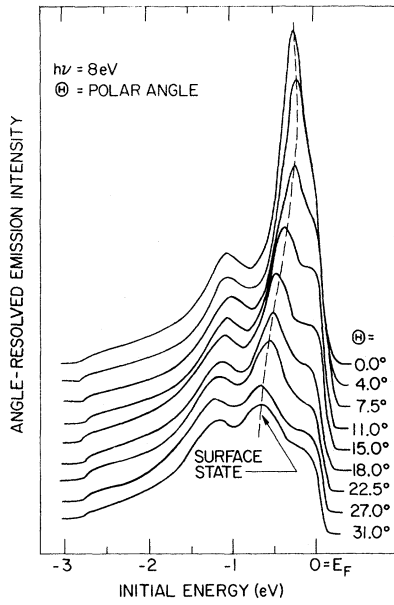


FIG. 2. Angle-resolved energy distributions as a function of emission direction  $\theta$  in the  $\{11\bar{2}\}$  plane showing surface-state dispersion. The relative intensities have been normalized to the lowest peak ( $\Lambda_1$  band).

(equivalently, with momentum perpendicular to the surface,  $k_{\perp}$ ).

AREDC's are presented in Fig. 2 which show that the surface state disperses downwards with increasing parallel momentum  $\vec{k}_{\parallel}$  ( $|\vec{k}_{\parallel}| \propto E^{1/2} \sin\theta$ , where  $\theta$  is the polar angle of emission). Since the surface-state emission intensity is strongly damped off normal, transitions from the bulk Ni bands near  $E_F$  become more visible (e.g., at  $-0.2$  eV for  $\Theta = 27^\circ$ ). These bulk states disperse with  $\vec{k}_{\parallel}$  less than the surface state, and remain when the intrinsic surface state is removed by an adsorbate. For example, a bulk state at  $-0.2$  eV is seen in Fig. 1 (curve c) which is nearly degenerate with the surface state. In Fig. 3, we summarize the energy dispersion of the surface state as well as of two bulk states near  $L$ . We observe two bulk transitions which start at initial energies of  $-0.15$  and  $-0.9$  eV below  $E_F$ , respectively, near threshold and move to lower initial energies with increasing photon energy. The upper state was studied with the surface state removed by 0.06 monolayers of oxygen (also hydrogen or CO); the lower state was determined from clean Ni(111) spectra. The final energy  $E$  above  $E_F$  is related to the wave vector  $k_{\perp}$  in a simple way for normal emission from the  $\langle 111 \rangle$  surface: According to band-structure calculations, there

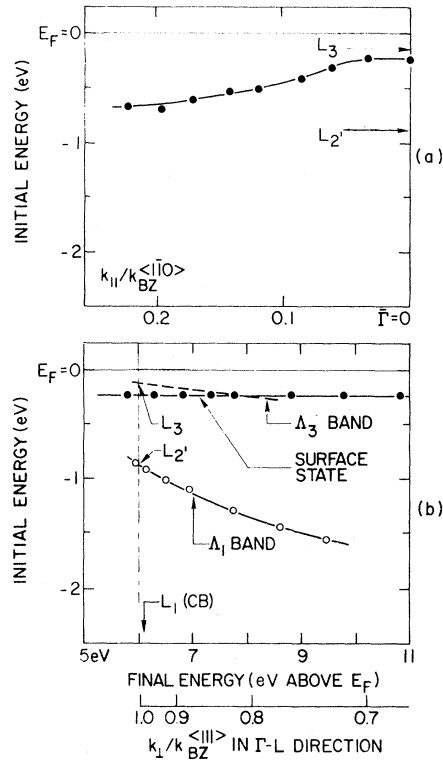


FIG. 3. (a) Dispersion of the surface state with parallel momentum  $\vec{k}_{\parallel}$  in the  $\langle 1\bar{1}0 \rangle$  direction ( $k_{BZ} \langle 1\bar{1}0 \rangle = 1.68 \text{ \AA}^{-1}$  = zone boundary). (b) Dispersion of the surface state and two bulk bands near  $L$  with excitation energy. The  $k_{\perp}$  momentum scale has been derived from the conduction band of Ref. 7, which was shifted down by 0.5 eV to make the conduction-band minimum  $L_1$  coincide with our experimental value ( $L_1 \approx 6.1$  eV).

is a single parabolic conduction band in the  $\Gamma-L$  direction which starts near the vacuum level at the  $L$  point and moves monotonically towards higher energy as  $k_{\perp}$  moves from  $L$  to  $\Gamma$ . The  $k_{\perp}$  scale in Fig. 3 is based on this band.<sup>7</sup>

For an assignment of initial-state symmetries in Fig. 3(b), we use polarization selection rules as described by Hermanson<sup>8</sup> which we have found to be valid for Cu(111). The only surface (and bulk) state which can be seen in normal emission for Ni(111) must have either  $\Lambda_1$  or  $\Lambda_3$  symmetry, which are excited with the electric field vector  $\vec{E}$  polarized parallel and perpendicular to the surface, respectively.<sup>8</sup> The  $\Lambda_3$  band is enhanced by  $s$ -polarized light ( $\vec{E} \parallel$  surface), whereas the  $\Lambda_1$  band and the surface state are enhanced by  $p$ -polarized light ( $\vec{E}$  close to sample normal). Thus, the surface state must have  $\Lambda_1$  symmetry. Moreover, the surface state lies in a  $\Lambda_1$ -symmetry gap above the top of the observed  $\Lambda_1$  bulk band.

Band calculations show that the top of the  $\Lambda_3$  and  $\Lambda_1$  bulk bands of interest have  $L_3$  and  $L_2'$  symmetries, respectively. The  $L_3$  level lies below  $L_2'$  in Cu whereas we observe the opposite for Ni. As a result, the bulk bands joining  $L_2'$  disperse upward with increasing  $\vec{k}_{\parallel}$  (toward  $W$ ,  $K$ , etc.) in Cu but disperse downward for our Ni band topology. The latter is identical, e.g., to that of the minority bands in Callaway and Wang.<sup>9</sup> Since the Cu(111) surface-state dispersion tracks this bulk band, one expects the same behavior for Ni(111), as we in fact observe.

The existence of a surface state in the  $\Lambda_1$ -symmetry gap above  $L_2'$  is common to the  $\langle 111 \rangle$  surfaces of the noble metals Cu, Ag, and Au.<sup>10,11</sup> To characterize the Ni(111) surface state further, we have measured the angle-resolved  $h\nu$ -dependent photoionization cross section for the surface state relative to the bulk emission cross section for Ni(111) and Cu(111) under the same conditions. The ratios of surface-state to bulk photoemission intensity are shown in Fig. 4. For Ni(111), there is emission from the  $\Lambda_3$  band that overlaps the surface emission; therefore, we have used difference spectra such as curves *c* and *d* in Fig. 1 to determine the surface and bulk  $d$ -band emission intensities. As seen in Fig. 4, the relative cross sections for the Cu and Ni surface states are very similar, both decreasing very rapidly with increasing photon energy. This behavior is similar to the behavior of bulk  $s$ - $p$ - vs  $d$ -state cross sections.<sup>12</sup> A recent *ab initio* calculation<sup>13</sup> for Pd(111) gives a  $\Lambda_1$  surface state which is analogous to the Ni(111) surface state and has predominantly  $s$ - $p_z$  character.

In summary, our assignment of bulk bands

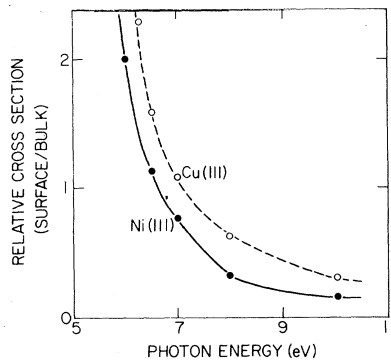


FIG. 4. The ratio of surface to bulk emission intensity (normal emission) for the Ni(111) and Cu(111) surface states.  $P$ -polarized radiation is incident  $60^\circ$  from normal.

differ markedly from recent band calculations,<sup>5,6,9</sup> with  $L_3$  and  $L_2'$  inverted in order and with  $L_2'$  being much lower than calculated. Our value for  $L_3$  is compatible with an exchange splitting  $\delta E_{ex} < 0.5$  eV and, if we associate  $L_3$  with the majority band ( $\Delta \approx 0.15$  eV), its proximity to  $E_F$  is compatible with both the observed sign change in spin-polarized photoemission<sup>2</sup> just above threshold<sup>3</sup> and the Stoner continuum gap  $\Delta \approx 0.075$  eV. Namely, the transition to positive spin polarization takes place at about  $2\Delta$  above threshold because of the high density of majority spins near  $L_3$ .<sup>3</sup> The  $\Lambda_1$  surface state affects photoemission (especially spin-polarized), field-emission, chemisorption, and ion-neutralization properties of Ni(111). For example, the large surface-state photoemission near threshold (see Fig. 4) is essentially nonmagnetic (based on calculated  $s$ - $p$  bands) and affects the magnitude of the spin polarization. Tunneling from the tail of the surface state at  $E_F$  explains the low spin polarization in field emission from Ni(111) ( $< 3\%$ )<sup>14</sup> in the absence of  $sp$  bulk bands at  $E_F$ . Strong  $s$ - and  $p$ -electron adsorbate bonding interactions (relative to  $d$ -electron effects) have been reported<sup>15</sup> for Ni(111); these are likely due in part to the intrinsic Ni(111) surface state reported here.

We wish to acknowledge the excellent support of the Synchrotron Radiation Center and the many contributions of J. J. Donelon and A. Marx. This work was supported in part by the U. S. Air Force Office of Scientific Research under Contract No. F 44620-76-C-0041.

<sup>1</sup>P. Heimann and H. Neddermeyer, J. Phys. F **6**, L257 (1976).

<sup>2</sup>W. Eib and S. F. Alvarado, Phys. Rev. Lett. **37**, 444 (1976).

<sup>3</sup>E. P. Wohlfarth, Phys. Rev. Lett. **38**, 524 (1977).

<sup>4</sup>D. G. Dempsey and L. Kleinman, Phys. Rev. Lett. **39**, 1297 (1977).

<sup>5</sup>C. S. Wang and J. Callaway, Phys. Rev. B **9**, 4897 (1974).

<sup>6</sup>C. S. Wang and J. Callaway, Phys. Rev. B **15**, 298 (1977).

<sup>7</sup>V. Moruzzi, private communication.

<sup>8</sup>J. Hermanson, Solid State Commun. **22**, 9 (1977).

<sup>9</sup>J. Callaway and C. S. Wang, Phys. Rev. B **7**, 1096 (1973).

<sup>10</sup>P. O. Gartland and B. J. Slagsvold, Phys. Rev. B **12**, 4047 (1975).

<sup>11</sup>P. Heimann, H. Neddermeyer, and H. F. Roloff, J. Phys. C **10**, L17 (1977).

<sup>12</sup>D. E. Eastman, in *Proceedings of the Fourth International Conference on Vacuum Ultraviolet Radiation Physics, Hamburg, 1974*, edited by E. E. Koch, R. Haensel, and C. Kunz (Pergamon, New York, 1974), p. 417. Relative differences in the energy-dependent

mean free paths in Cu and Ni are much smaller than the energy dependence in Fig. 4.

<sup>13</sup>S. G. Louie, *Phys. Rev. Lett.* **40**, 1525 (1978).

<sup>14</sup>M. Landolt, private communication.

<sup>15</sup>J. E. Demuth, *Surf. Sci.* **65**, 369 (1977).

## Single-Rayleigh-Phonon Interaction in the Scattering of He from LiF(001)

James M. Horne and David R. Miller

*Department of Applied Mechanics and Engineering Sciences, University of California, San Diego, La Jolla, California 92093*

(Received 22 May 1978)

Energy analysis has been performed on 63-meV He atoms scattered from 135°K LiF(001) along the <010> direction. The results suggest that single Rayleigh phonons dominate the interaction near specular scattering. Points on the dispersion curve are determined uniquely and suggest a limiting speed of sound of  $(4.2 \pm 0.5) \times 10^5$  cm/sec.

Since the early work of Cabrera, Calle, and Manson<sup>1</sup> on inelastic scattering of atoms by crystal surfaces it has been hoped that atomic-beam scattering could provide useful information about surface-phonon spectra. It appears at this time that an ideal coupling of such experiments with a rigorous theory may only be accomplished in the limit of single-phonon processes. Experiments to date have only reported scattered angular intensity distributions. The most interesting cases have shown intensity maxima and/or minima in the inelastic scattering about specular or diffraction peaks for LiF(001),<sup>2,3</sup> Ag(111),<sup>4</sup> and Au(111).<sup>5</sup> Several types of analysis exist for these structures<sup>2,2,6-10</sup> using various approximations. For example, one type of important simplification is to assume a flat surface, conserving tangential momentum, or at another limit, to assume only Rayleigh phonons are involved so that the phonon only transfers tangential momentum. We have felt that appropriate approximations will only be substantiated when both energy and angular distributions can be made in a regime where single-phonon interactions are dominant. Under these conditions the ideal beam scattering experiment can uniquely determine the frequency ( $\omega$ ) and surface tangential momentum vector ( $\bar{Q}$ ) of the phonon involved. In this Letter we report the first such experiment. We feel the data indicate an interaction dominated by a single-Rayleigh-phonon process. We first review the kinematics involved for our type of experiment.

For a single-phonon process, associated with the specular peak, which scatter in the plane of the incident beam and the surface normal, i.e.,

the phonon travels in plane, the conservation laws can be written

$$k_s \sin \theta_s = k_i \sin \theta_i + \left( \frac{G}{L} \right) Q, \quad (1a)$$

$$k_s^2 = k_i^2 + \left( \frac{A}{C} \right) \frac{2m\omega}{\hbar}, \quad (1b)$$

where  $\theta$  is measured from the surface normal and  $\omega$  and  $Q$  are taken as positive scalar quantities. The symbols  $G = +1$  and  $L = -1$  represent gain or loss of parallel momentum, since the phonon can travel in either direction, and  $A = +1$  and  $C = -1$  represent annihilation and creation of the phonon, respectively. Equations (1a) and (1b) can be combined to eliminate  $k_s$  and give a simple relationship  $\omega = \omega(Q, k_i, \theta_i, \theta_s, m)$ . Therefore, with a specified incident particle ( $k_i, \theta_i, m$ ), at each in-plane scattered angle,  $\theta_s$ , there are four unique curves of  $\omega = \omega(Q)$  along which the solution for a particular phonon interaction must lie if it is to satisfy the conservation Eqs. (1a) and (1b). Figure 1 shows a plot of such solutions for a sub-specular scattering. The case (C, G) yields no positive  $\omega$  solution so that these processes are not permitted for the specified conditions. The possible scattering solutions are now given by the intersection of these curves with the dispersion curves for a particular crystal surface of interest. For illustrative purposes, a hypothetical set is shown as dashed curves in Fig. 1. We have used the nomenclature and qualitative features of the calculations of Allen, Alldredge, and DeWette<sup>11</sup> for a model which should represent LiF reasonably well; these are not computed curves for LiF, however.